

## Article

# Dynamic Assessment of the Structural Behavior of a Pedestrian Bridge Aiming to Characterize and Evaluate Its Comfort Level

Reina El Dahr \*, Xenofon Lignos, Spyridon Papavieros and Ioannis Vayas

Institute of Steel Structures, National Technical University of Athens, 15772 Athens, Greece;  
vastahl@central.ntua.gr (I.V.)

\* Correspondence: rdahr@mail.ntua.gr

**Abstract:** The assessment of infrastructure integrity is considered paramount to verify its structural health and to build its resilience. In this study, a monitoring strategy, consisting of a pre-developed microcontroller-based data acquisition system (DAQ) hardware and a software program for post processing built on LabVIEW platform, was conducted to assess the structural behavior of an arch-and-tie pedestrian bridge located in Haidari, Greece, following its construction phase. This endeavor aimed to delineate its systemic state and to verify the fulfillment of comfort criteria stated by EN1990, HIVOSS and SETRA guidelines. To this end, four trademark Bridge Diagnostic Inc. (BDI) triaxial accelerometers were meticulously deployed along the bridge expanse to scrutinize the structure's response toward a spectrum of induced perturbations. The established framework effectively compiled the acquired acceleration time domain then employed a Butterworth bandpass filter to derive the bridge eigenfrequencies, eigenmodes, and damping ratios. The resultant findings conclusively indicate that the bridge response towards pedestrian crossing conforms to the established specifications and thus does not necessitate the installation of dampers. The bridge maintains comfortable structural integrity for pedestrian traversal up to an upper frequency limit of 3.67 Hz, substantiating its ability to absorb the dissipated energy generated by pedestrian movement.

**Keywords:** structural health monitoring; bridge assessment; comfort level characterization; damping; eigenfrequency; LabVIEW



**Citation:** El Dahr, R.; Lignos, X.; Papavieros, S.; Vayas, I. Dynamic Assessment of the Structural Behavior of a Pedestrian Bridge Aiming to Characterize and Evaluate Its Comfort Level. *Buildings* **2023**, *13*, 3053. <https://doi.org/10.3390/buildings13123053>

Academic Editors: Shaohong Cheng and Haijun Zhou

Received: 20 November 2023

Revised: 29 November 2023

Accepted: 3 December 2023

Published: 7 December 2023



**Copyright:** © 2023 by the authors. Licensee MDPI, Basel, Switzerland. This article is an open access article distributed under the terms and conditions of the Creative Commons Attribution (CC BY) license (<https://creativecommons.org/licenses/by/4.0/>).

## 1. Introduction

In pursuit of meeting architectural requirements, engineers often aim to design elongated-spanned pedestrian bridges, and to adopt lightweight yet high-strength materials [1]. This innovation considerably lowers the eigenfrequency of the footbridge, which in return renders the structure more vulnerable to oscillations, resulting in the discomfort of pedestrians when crossing the bridge [2]. Nonetheless, the amount of reported bridge harm has dramatically escalated, along with increased complaints about the deterioration state, following the expansion of service duration and the high traffic loads bridges are subjected to [3]. In such a situation, it becomes crucial to give priority to any infrastructure for renovation and restoration depending on its assessed health [4].

Ongoing development in bridge design and construction, coupled with advancements in assessment techniques, has highlighted the importance of monitoring its performance from the construction phase through operation and maintenance for safety and comfort characterization [5]. Therefore, assessing a bridge's health has emerged to prevent any adverse event that may befall the structure [6–11]. In their 2001 research, Peeters et al. classified the aspects that could harm a bridge, such as metal corrosion and material aging, resulting in strength loss. Furthermore, any externally induced disturbance has a significant impact on the vibrational evaluation of bridges. Among these, the system can be stimulated by the crowd standing atop the structure, the force of the wind, and the vibrations induced at the base of the structure [12]. Consequently, dynamic assessment is conducted to evaluate

vibrational properties intending to certify its design safety, analyze the health state, and detect any harmful deterioration [13–16]. The most crucial vibrational characteristics to assess are eigenfrequencies, eigenmodes, and damping ratios [17,18]. Pirskawetz and Schmidt, in 2023, evaluated the structural response of a prestressed concrete bridge located in Germany after being exposed to acoustic emission through destructive tests to detect wire breakage [19]

As a result, modal analysis is established in assessing the dynamic behavior of structures [20–23]. Thus, operational modal analysis (OMA) is particularly employed in health-monitoring strategies, deemed to evaluate modifications in the framework vibrational measurements [24,25]. Gonzalez et al., in 2023, proposed a power spectral density-based algorithm for bridge monitoring purposes within vehicle measurements. It was able to identify, localize, and assess single cracks on a 15 m span simply supported bridge [26]. In this study, we have adopted an operational modal testing procedure to estimate the dynamic measurements of a pedestrian bridge by inducing perturbations at various positions along the bridge.

The operational lifespan of a pedestrian bridge is intricately tied to the influence of individuals traversing it, mainly the number of people crossing, their activities, and the duration of their presence on the bridge [27], resulting in modifications to its dynamic aspect and modal attributes. Generally, pedestrians exhibit a proclivity for coordinated interactions while crossing a bridge in order not to intersect. Therefore, this human–human interface results in modifying their paths. Accordingly, neighbor pedestrians adjust their walking cadence to harmonize with those around them [28]. Furthermore, the human–structure interface may generate a discomfort for pedestrians when crossing a bridge, since their walking frequencies tend to match with the bridge’s motion causing a resonance oscillation state. Dallard et al. referred to this encounter impact as the “lock-in phenomenon” ([29], p. 413).

Pedestrian bridges experience not only vertical vibrations caused by dynamic forces induced by crowd movement, but also significant lateral vibrations, as exemplified by the unexpected lateral oscillations that arose in the London Millennium Footbridge [30]. These movements were triggered by a significant lateral loading effect, a factor that was not initially foreseen during the design phase and had received limited prior investigation.

In the realm of bridge dynamics, evaluating the system response toward an induced stimulation indicates that the bridge oscillation may reach an uncomfortable state for pedestrians, and so it becomes imperative to implement a vibration absorbent framework for the undesirable bridge motion.

Passive damping mechanisms such as tuned mass dampers (TMDs) are adopted on structures that are vulnerable to oscillation, such as pedestrian bridges, stadiums, or high-rise building constructions. When it comes to the advancement of damping systems, bridges, regardless of their specific design, offer a fascinating area of investigation [31]. TMDs have proven valuable not only in the design of new structures, but, also, they are implemented on existing ones. Moreover, they come with a decent maintenance price [32]. Caetano et al. [33,34] conducted a study on the Pedro e Inés bridge in Coimbra, Portugal, focusing on the structure oscillation caused by pedestrians while crossing the bridge. Their research involved extended monitoring to analyze the bridge dynamic behavior and the implementation of tuned mass dampers (TMDs) to mitigate vertical and lateral vibrations.

In this study, a monitoring methodology was conducted, aiming to assess the structural behavior and verify the fulfillment of the comfort criteria of the Haidari pedestrian bridge located in Greece after the completion of its construction.

## 2. Comfort Level of Pedestrian Bridges

In the present work, the emphasis on pedestrian comfort is gaining significant consideration in both the design and functionality evaluations of footbridges. Prioritizing the comfort of individuals when crossing a footbridge is of utmost importance, given the multifaced challenge this issue may present. The comfort of individuals traversing a

pedestrian bridge is influenced by a range of subjective factors, among them the ambient noise, traffic volume on the bridge, bridge elevation from the ground, and the aspect of the people crossing themselves. In 2016, Tubino et al. carried out an extensive experimental study on two well-utilized footbridges located Italy. The design objectives were set in accordance with the bridge owner's specifications, focusing on achieving both the average and the ultimate comfort stage [35].

It is widely acknowledged that vibrational acceleration stands as the primary influencing factor affecting pedestrian comfort [36]. In previous investigations, researchers primarily focused on the impact of vibrational magnitude and velocity on experienced comfort [37–39]. Nevertheless, as research has progressed in examining human experiences in their surroundings, there is a consensus among scholars that this comfort is chiefly governed by the dynamic acceleration experienced over time, rather than velocity. In their 2017 study, Dey et al. assessed various design protocols using data obtained from tests conducted on two real-time pedestrian bridges. Their findings indicated that the protocol typically defines comfort thresholds based primarily on acceleration [40].

ISO 2631-1 [41] categorized the pedestrians' comfort limits into six distinct groups aligned with various acceleration amplitudes, and several recent studies have embraced this comfort partition [42]. Similarly, alternative standards, such as the European HIVOSS guideline from 2008 [43] and the French guideline Sétra from 2006 [44], have outlined acceleration associated with specific comfort levels, as highlighted by Van Nimmen et al. in 2014 [45].

This research presents the evaluations of the vibrational performance of the Haidari pedestrian bridge, with the goal of characterizing its structural condition and emphasizing the pedestrian's comfort. This approach is grounded in the correlation between pedestrians' comfort and the highest acceleration experienced on the footbridge.

### 3. Case Study

A monitoring strategy was conducted aiming to assess the structural behavior and the comfort of Haidari pedestrian bridge located in Greece after the completion of construction. The structure is an arch-and-tie bridge with a span length of 44.6 m and width of 2.74 m. Along one side, the arch stands in an eccentrical position connected to six PFEIFER type PV115 wire cables, as shown in Figure 1. The concrete deck is supported by steel girders-cantilevers of variable trapezoidal profile sections which are connected to the arch element. The bridge rests on two pedestals situated atop piles. The measured total dead weight of the bridge is 152 tons.



**Figure 1.** Cross-section of Haidari pedestrian bridge.

Four triaxial BDI accelerometers were strategically placed along the bridge to monitor time-varying oscillations. A predefined sensor placement was suggested in accordance with the areas on the deck expected to experience the most significant disturbances, deemed as the optimal sensor placement. Specifically, two sensors were deployed at the midpoint of the bridge, one on the cantilever section, and one adjacent to the bow. The remaining two

sensors were positioned at the quarter-span, near the edge of the cantilever, as illustrated in Figure 2. These sensors recorded accelerations in the vertical (z), longitudinal (x), and transversal (y) directions along the bridge deck. Subsequently, the sensor data were transmitted via wiring to a control unit located outside the bridge structure. The spatial arrangement of these sensors in a top-down view is illustrated in Figure 3. The sensor network was connected to a data acquisition system in order to process and evaluate the recorded vibrational signals collected by the accelerometers.

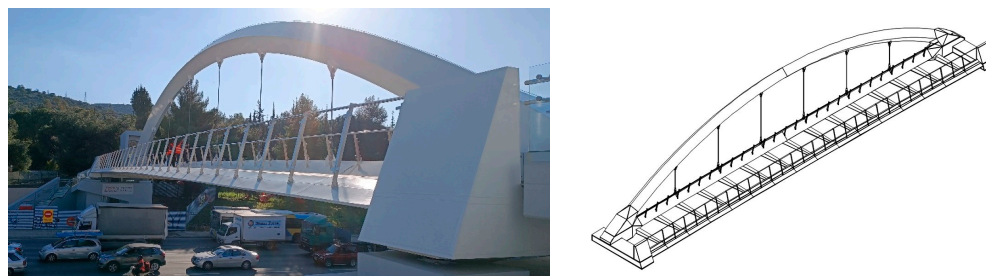


Figure 2. Side view of Haidari pedestrian bridge.

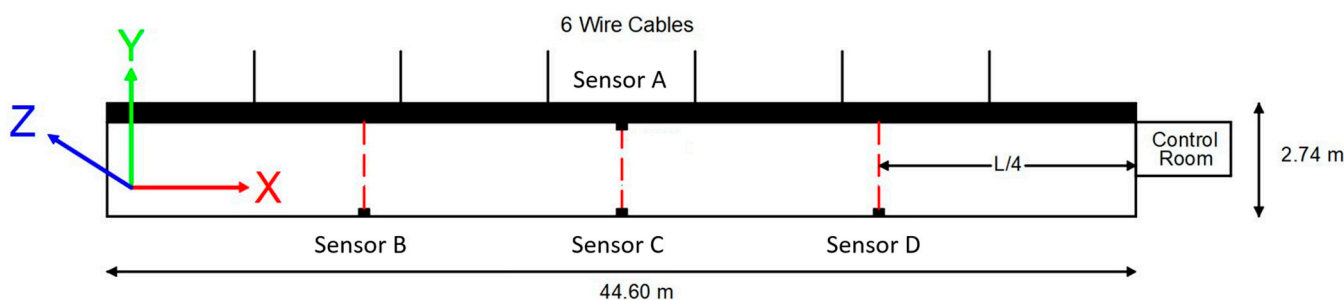


Figure 3. Sensor network mounted on Haidari pedestrian bridge.

The adopted DAQ system was designed and validated by El Dahr et al. in 2022 [46]. It is a microcontroller-based, accurate, and low-cost acquisition framework that facilitates the aggregation and analysis of gathered data, relying on a Teensy 4.1 digital microcontroller of a resolution of 32 bits to execute these operations. Along with its PC computer, it was employed to receive the data and calculate the output through a programming software such as MATLAB or LabVIEW.

In this study, the results were computed using a LabVIEW programming platform developed by El Dahr et al. in 2023 [47]. LabVIEW, which stands for Laboratory Virtual Instrument Engineering Workbench, is a graphical user interface-based programming tool predominantly employed for data acquisition and structural assessment. One of the primary advantages of this approach is its well-defined conceptual framework, enabling the calculation of modal properties and reducing computational complexity while facilitating its versatile application in various projects, such as bridges, towers, and tall structures. Furthermore, its network of sensors and topological architecture ensures superior precision in data collection and an optimized strategy for analysis when compared to other data acquisition (DAQ) methodologies.

#### 4. Experimental Procedure

The aim of the study was to observe how the system responds to various external disturbances in order to estimate the dynamic characteristics of the bridge under scrutiny, characterizing the comfort level experienced by pedestrians when crossing the bridge. Therefore, the investigations were conducted in two distinct phases.

The first phase was intended to calculate the bridge eigenfrequencies, damping ratios, and eigenmodes. This was achieved through the application of controlled excitations, with

a particular focus on inducing vertical and lateral oscillations. These disturbances were initiated by both cases, an individual and a group of people, who, through rhythmical bouncing actions, excited the bridge within its natural frequency spectrum. These jumping events predominantly occurred at positions corresponding to 1/2 and 1/4 of the bridge's length. Rhythmic activities encompassed an impact vertical jump with landing on two feet, and hops from one leg to the other were performed to induce vertical and horizontal oscillations, respectively. The pedestrians complied with the rhythm of a tone generator. The frequency of foot-to-foot jumps was 3.67 Hz, which from preliminary measurements had given the first vertical eigenfrequency of the bridge, with 2.0 Hz corresponding to normal walking. The jumps stopped abruptly after reaching a level of oscillations and the free response of the carrier until rest was measured. The set of Stage 1 tests is presented in Table 1.

**Table 1.** Protocol of imposed stimulations of Phase 1 tests.

Pedestrian: Mass [Kg]	Position	Type/Frequency
A: 80.9 Kg B: 94.8 Kg C: 103.6 Kg	0.5 L	Impact Jump
	0.5 L	3.67 Hz foot to foot
	0.5 L	2 Hz foot to foot
	0.25 L	Impact Jump
	0.25 L	3.67 Hz foot to foot
	0.25 L	2 Hz foot to foot
Six Pedestrians: 543.1 Kg	0.5 L	Impact Jump
	0.5 L	3.67 Hz foot to foot
	0.25 L	Impact Jump
	0.25 L	3.67 Hz foot to foot

The second phase of testing was aimed at assessing whether the pedestrian bridge conformed to the requisite standards for oscillation comfort during pedestrian transit. Data acquisition involved recording the movements of one pedestrian and a crowd of nine people walking on a predefined path for specific frequencies.

The traffic on the bridge is classified between very light and light according to HIVOSS guidelines [43] and SETRA [44], since the bridge is located in an urban area that can be occasionally loaded, with a pedestrian density of 0.1–0.2 pedestrian/m<sup>2</sup>.

Three different types of gait characteristics of walking, running, and random walking, where each pedestrian walked at their own pace, were tested for the intentional stimulation of the subject. The recording of accelerations in all crossings started 10 s before the beginning of pedestrian movement on the bridge deck and ended 20 s after they stopped. The set of examined crossings for one pedestrian and for a group of nine pedestrians is given in Table 2.

**Table 2.** Protocol of imposed stimulations of Phase 2 tests.

Pedestrian: Mass [Kg]	Type/Frequency	Path
A: 80.9 Kg B: 94.8 Kg C: 103.6 Kg	2.0 Hz Walk 3.67 Hz Walk Random Walk	
Nine Pedestrians: 791.2 Kg	2.0 Hz Walk 3.67 Hz Walk Random Walk	

## 5. Results and Interpretation

### 5.1. Acceleration Calculation

The DAQ system and the BDI accelerometers have a sampling frequency of 200 Hz. Accelerometers along the bridge were recording raw data in response to external

disturbances. The LabVIEW code was employed to compute and eliminate the mean value from the recorded acceleration, thereby mitigating the offset inherent in the raw acceleration–time graph. The removal of this offset is crucial to minimize potential sources of error. To derive the corrected acceleration–time domain, the mean value is subtracted from the raw acceleration–time domain. The structure is designed to experience a maximum acceleration of  $0.7 \text{ m/s}^2$  in the vertical direction and  $0.2 \text{ m/s}^2$  in the lateral direction.

An evaluation of pedestrian A leaping at the bridge's midpoint is provided in the paragraphs that follow. Figure 4 shows the corrected acceleration time domain collected by accelerometer A recording the structural response toward pedestrian A disturbing the bridge with an impact jump at the mid-length of the bridge. The results are presented in the vertical direction. The mean value was determined to be  $9.8049 \text{ m/s}^2$  and was subtracted. The highest acceleration recorded was  $0.92 \text{ m/s}^2$  reported at  $8.15 \text{ s}$  when the bridge was disturbed. The acceleration is higher than the maximum allowable acceleration in the vertical direction of  $0.7 \text{ m/s}^2$  that the bridge is originally designed to experience, causing a discomfort feeling for a  $1 \text{ s}$  period of time.

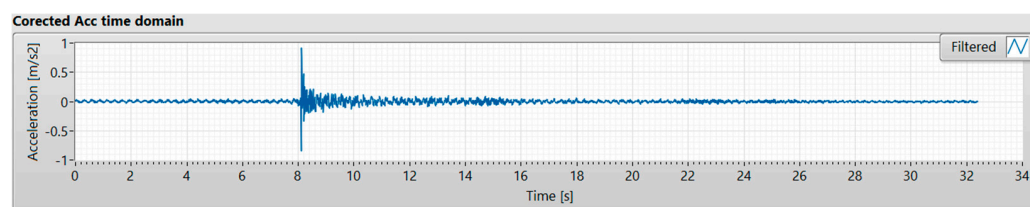


**Figure 4.** Corrected acceleration–time domain of accelerometer A for pedestrian A in vertical direction.

Figure 5 shows the corrected acceleration time domain collected by accelerometer A recording the structural response toward pedestrian A disturbing the bridge with an impact jump at the mid-length of the bridge. The results are presented in the lateral direction. The mean value was determined to be  $-0.27864 \text{ m/s}^2$  and was retrieved. The highest acceleration recorded was  $0.16 \text{ m/s}^2$ , reported at  $8.15 \text{ s}$  when the bridge was disturbed. The acceleration is lower than the maximum allowable acceleration in the lateral direction of  $0.2 \text{ m/s}^2$ , which the bridge is originally designed to experience.

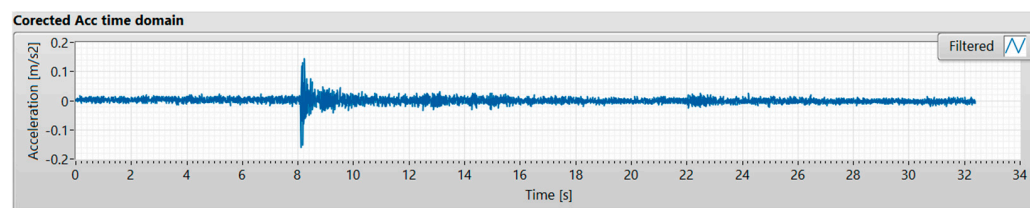


**Figure 5.** Corrected acceleration–time domain of accelerometer A for pedestrian A in lateral direction.

Figure 6 shows the corrected acceleration time domain collected by accelerometer A recording the structural response toward the six pedestrians disturbing the bridge with an impact jump at the mid-length of the bridge. The results are presented in the vertical direction. The highest acceleration recorded was  $0.6 \text{ m/s}^2$  reported at  $13.3 \text{ s}$  when the bridge was disturbed. The acceleration is lower than the maximum allowable acceleration in the vertical direction of  $0.7 \text{ m/s}^2$ , which the bridge is originally designed to experience.

Figure 7 shows the corrected acceleration time domain collected by accelerometer A recording the structural response toward the six pedestrians disturbing the bridge with an impact jump at the mid-length of the bridge. The results are presented in the lateral direction. The highest acceleration recorded was  $0.25 \text{ m/s}^2$  reported at  $13.3 \text{ s}$  when the bridge was disturbed. The acceleration is higher than the maximum allowable acceleration in the lateral direction of  $0.2 \text{ m/s}^2$ , which the bridge is originally designed to experience, causing a discomfort feeling for a  $1 \text{ s}$  period of time.

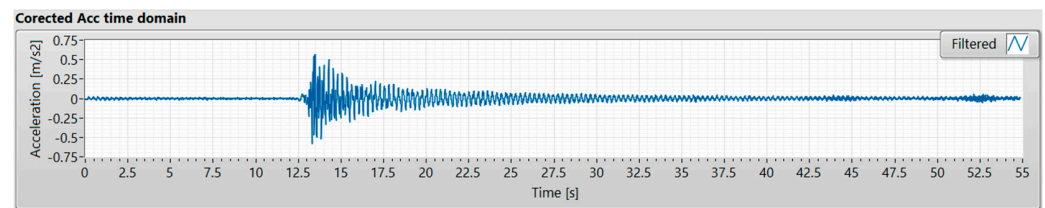


Figure 6. Corrected acceleration–time domain of accelerometer A for 6 pedestrians in vertical direction.

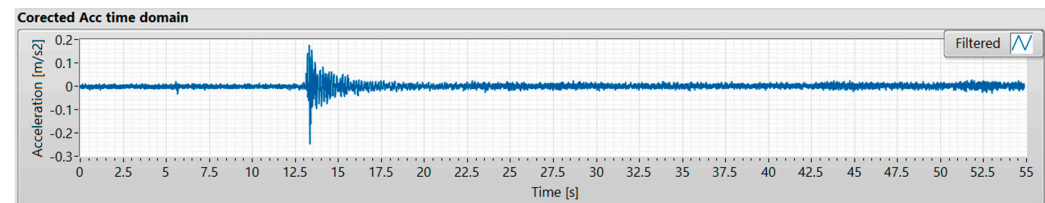


Figure 7. Corrected acceleration–time domain of accelerometer A for 6 pedestrians in lateral direction.

### 5.2. Natural Frequencies

Determining the eigenfrequencies of a pedestrian bridge is useful to inspect its sensitivity to oscillations during pedestrian crossing. Indeed, if a structure's eigenfrequencies are close to the eigenfrequencies of pedestrian traffic, there is a risk of resonance. The critical eigenfrequency intervals according to the EN 1990 standard [48] and the SETRA [44] and HIVOSS [43] guidelines are given in Table 3.

Table 3. Frequency ranges with resonance risk.

Coordination Risk	Frequency [Hz]					
	Vertical Oscillations			Lateral Oscillations		
	EN 1990	HIVOSS	SETRA	EN 1990	HIVOSS	SETRA
Negligible	>5	<1.25 >4.6	<1.0 >5.0	>2.5	<0.5 >1.2	<0.3 >2.5
Small			2.6–5.0			1.3–2.5
Medium	<5	1.25–4.6	1.0–1.7 2.1–2.6	<2.5	0.5–1.2	0.3–0.5 1.1–1.3
Big			1.7–2.1			0.5–1.1

The eigenfrequencies calculated in the designed phase (with contribution of the pedestrians mass with an estimation of 0.6 pedestrian/m<sup>2</sup>, for testing purposes, considering a pedestrian to be 0.8 kN) are as follows: 3.042 Hz, 7.76 Hz, and 10.28 Hz.

The frequency domain is obtained after performing power spectral density (PSD) function on the corrected acceleration time domain of accelerometer A in the vertical direction. The signal from PSD is evaluated to find the peaks in terms of natural frequencies in (Hz) and their respective power in  $\left[\frac{(\text{m/s}^2)^2}{\text{Hz}}\right]$  (Figure 8). It reports three eigenfrequencies, respectively, at 3.67 Hz, 7.62 Hz, and 10.22 Hz (Figure 9).

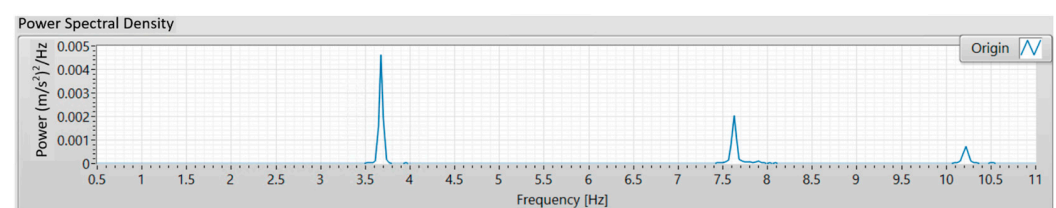
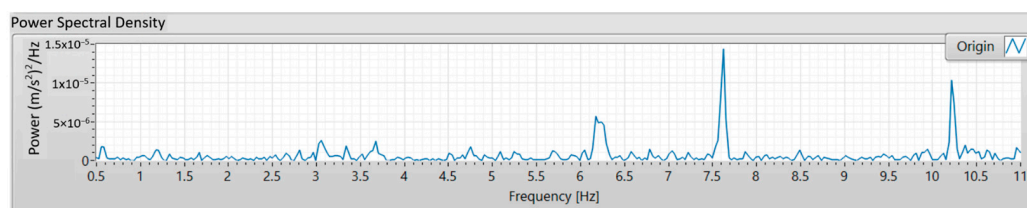


Figure 8. Power spectral density of the system eigenfrequency in vertical direction.

Eigenfrequencies	
3.6742	0.0046076
7.6261	0.0020377
10.218	0.00074054

**Figure 9.** Power spectral density with numerical inquiry of the system eigenfrequency in vertical direction.

The frequency domain is obtained after performing the power spectral density (PSD) function on the corrected acceleration time domain of accelerometer A in the lateral direction. The signal from PSD is evaluated in Figure 10 and reports three eigenfrequencies, respectively, at 3.67 Hz, 6.24 Hz, and 7.62 Hz (Figure 11).



**Figure 10.** Power spectral density of the system eigenfrequency in lateral direction.

Eigenfrequencies	
6.1839	0.0000059215
7.6223	0.000014445
10.225	0.000010649

**Figure 11.** Power spectral density with numerical inquiry of the system eigenfrequency in lateral direction.

The eigenfrequencies of the first two eigenmodes in the vertical and transverse directions, as well as their evaluation in terms of resonance risk, are given in Table 4.

**Table 4.** Bridge frequencies and comparison with resonant risk specifications.

Eigen Frequency	Frequency [Hz]		Coordination Risk					
	Vertical	Lateral	Vertical			Lateral		
			EN 1990	HIVOSS	SETRA	EN 1990	HIVOSS	SETRA
1st	3.67	6.18	Intermediate	Intermediate	Small	Negligible	Negligible	Negligible
2nd	7.62	7.62	Negligible	Negligible	Negligible	Negligible	Negligible	Negligible
3rd	10.22	10.22	Negligible	Negligible	Negligible	Negligible	Negligible	Negligible

### 5.3. Damping

The damping ratio was determined by LabVIEW through Hilbert transform for the eigenfrequencies of the bridge in both directions. It is estimated to be a maximum of 5% as per the original bridge design.

For the first eigenfrequency, a second-order Butterworth bandpass filter was applied on the corrected acceleration–time domain data of accelerometer A in the vertical direction, with cutoff frequencies between 3.61 and 3.73 Hz. According to the Hilbert transform, the damping ratio is 2.25% (Figure 12).

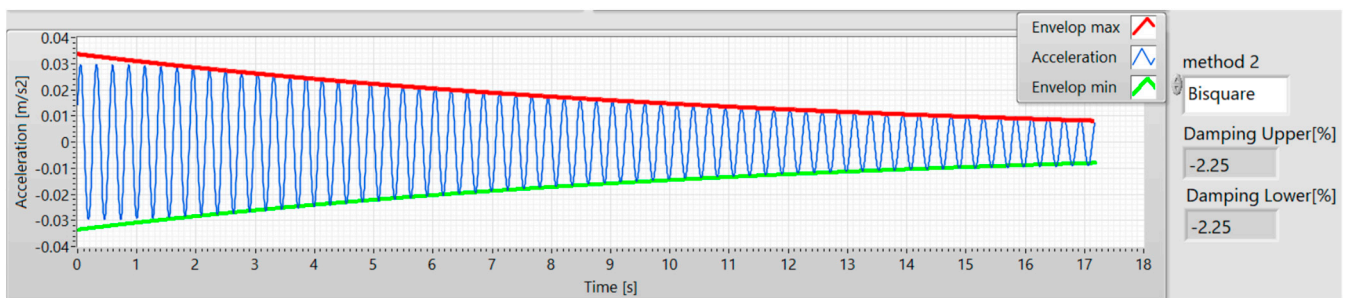


**Figure 12.** LabVIEW graph showing the acceleration–time domain of accelerometer A with envelopes for the first eigenfrequency in the vertical direction calculated by Hilbert transform.

For the second eigenfrequency, a second-order Butterworth bandpass filter was applied on the corrected acceleration–time domain data in the vertical direction, with cutoff frequencies between 7.56 and 7.68 Hz. According to Hilbert transform, the damping ratio is 1.45%. Same for the lateral direction, for the first eigenfrequency, a second-order Butterworth bandpass filter was applied on the corrected acceleration–time domain data, with cutoff frequencies between 6.1 and 6.2 Hz. According to the Hilbert transform, the damping ratio is 1.93%. For the second eigenfrequency in the lateral direction, a second-order Butterworth bandpass filter was applied on the corrected acceleration–time domain data, with cutoff frequencies between 7.56 and 7.69 Hz. According to Hilbert transform, the damping ratio is 1.14%. All four acceleration–time domains with envelopes for both eigenfrequencies in vertical and lateral directions calculated by Hilbert transform showed similar shapes.

Table 5 shows the system damping ratios for both eigenfrequencies in both directions.

**Table 5.** Damping ratios of the first 2 eigenfrequencies.

Eigenfrequency	Damping Ratio [%]	
	Vertical Direction	Lateral Direction
1st	2.25	1.93
2nd	1.45	1.14

The calculated damping ratios for the first and second eigenfrequencies in both directions satisfy the specified criteria, as they fall below the maximum allowable damping for which the bridge has been designed.

#### 5.4. Eigenmodes

Acceleration is proportional to displacement [49] since a double integration is needed to calculate displacement. Therefore, the mode shapes of the bridge can be pictured by reporting the filtered acceleration for each eigenfrequency.

For the first eigenfrequency, in the vertical direction the three accelerations delineated in blue dots along the bridge length (outlined in white) synchronize, having the same phase at a specific moment with a different altitude. From the reported data of the second eigenfrequency, both accelerometers installed on the quarter edges of the bridge share the same phase, yet the accelerometer mounted on the mid-length of the bridge is shifted by  $\pi/2$ . The amplitude of the accelerometers indicates the displacement aspect at each sensor location, revealing the two consecutive mode shapes of the bridge (represented in red) in Figures 13 and 14.

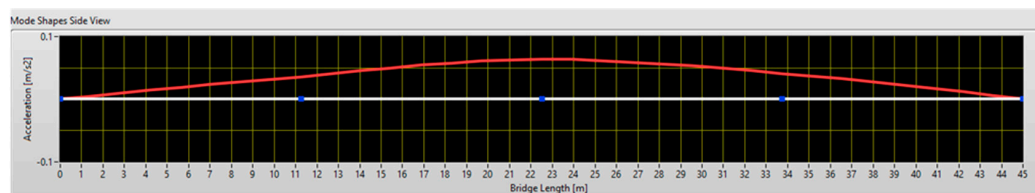


**Figure 13.** Bridge mode shapes in vertical direction for the first eigenfrequency.



**Figure 14.** Bridge mode shapes in vertical direction for the second eigenfrequency.

Likewise, for the first eigenfrequency in the lateral direction, the three accelerations delineated in blue dots along the bridge length (outlined in white) synchronize, having the same phase at a specific moment with a different altitude. From the reported data of the second eigenfrequency, both accelerometers installed on the quarter edges of the bridge share the same phase, yet the accelerometer mounted on the mid-length of the bridge is shifted by  $\pi/2$ . The amplitude of the accelerometers indicates the displacement aspect at each sensor location, revealing the two consecutive mode shapes of the bridge (represented in red) in Figures 15 and 16.

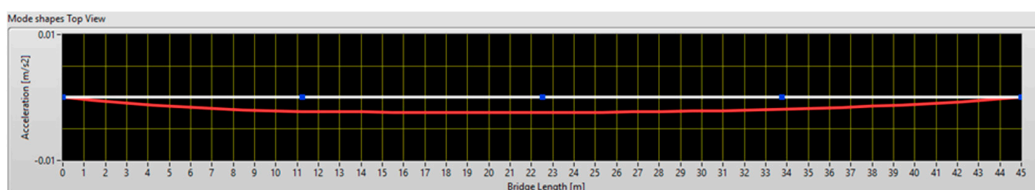


**Figure 15.** Bridge mode shapes in lateral direction for the first eigenfrequency.

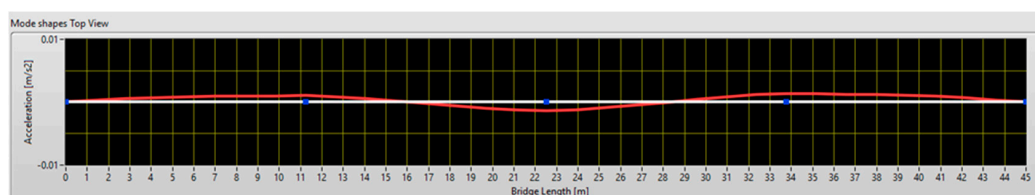


**Figure 16.** Bridge mode shapes in lateral direction for the second eigenfrequency.

In conclusion, it may be said that the analysis of the dynamic behavior of the tested pedestrian bridge after the completion of construction showed three eigenfrequencies of 3.67, 7.62, and 10.22 Hz for the vertical direction. A damping of 2.25% for the first and 1.45% for the second eigenfrequency were found. For the lateral direction, the three detected eigenfrequencies were 6.18, 7.62, and 10.22 Hz. And a damping of 1.93% for the first and 1.14% for the second eigenfrequency were found. For each eigenfrequency, a distinct mode shape was found.

### 5.5. Comfort Level

The second phase referred to finding the comfort levels for one pedestrian and a group of nine people. The activities of pedestrian A (80.9 Kg) and the group of nine pedestrians (791.2 Kg) were recorded when crossing the bridge through a predetermined path for a

2 Hz walk and a 3.67 Hz run and a random walk in both lateral and vertical directions. The comfort feeling was observed in pedestrians for all activities in the lateral and vertical directions. When crossing the bridge at 3.67 Hz, for the activity of one pedestrian, the comfort limits were touching the limit in the vertical direction, as is shown in Figure 17, but they were not surpassed. However, for the lateral direction, the pedestrian did not feel any structural movement causing their discomfort, as shown in Figure 18. Same for the activity of a group of pedestrians, the comfort limits were touching the limit in the vertical direction, as is shown in Figure 19, but they were not surpassed. However, for the lateral direction, the pedestrian did not feel any structural movement causing their discomfort, as shown in Figure 20.

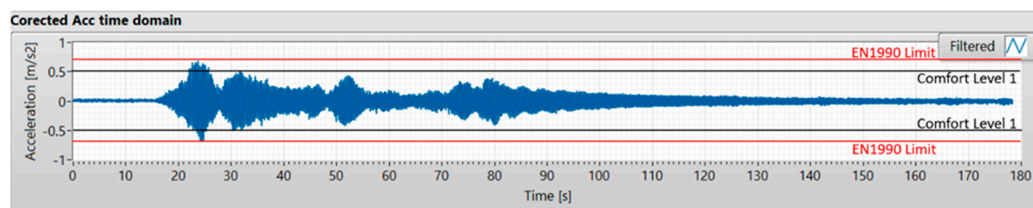


Figure 17. Comfort level for pedestrian A running at 3.67 Hz frequency in vertical direction.

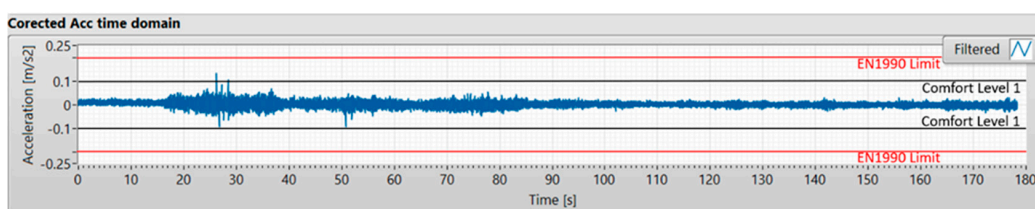


Figure 18. Comfort level for pedestrian A running at 3.67 Hz frequency in lateral direction.

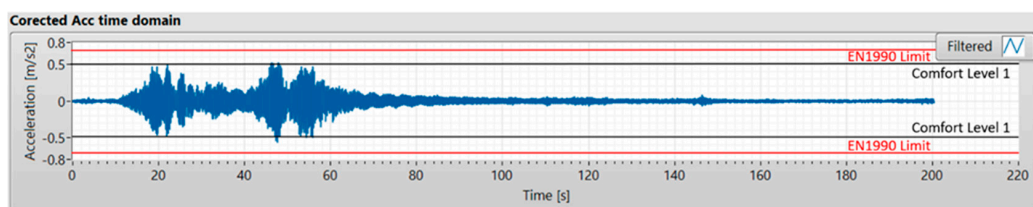


Figure 19. Comfort level of a 9-pedestrian group running at 3.67 Hz frequency in vertical direction.

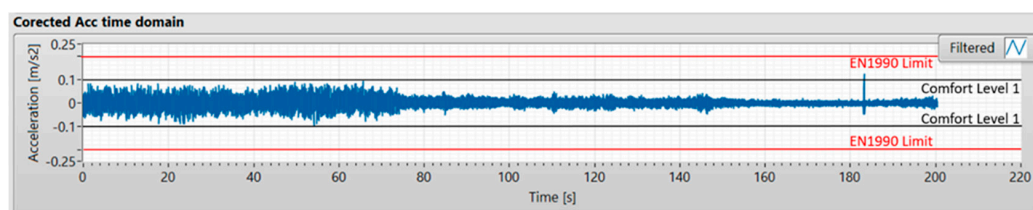


Figure 20. Comfort level of a 9-pedestrian group running at 3.67 Hz frequency in lateral direction.

The comfort standards are outlined in terms of maximum acceleration in EN 1990, A2.4.3.2 [48], and are as follows:

1. For vertical vibrations,  $0.7 \text{ m/s}^2$ .
2. For horizontal vibrations resulting from typical use,  $0.2 \text{ m/s}^2$ .

Comfortability does not have to reduce the bridge safety regulations, since damping calculations indicate and affirm having a safe structure. However, the movement of bridge is due to its capability of absorbing the energy produced by the pedestrian using it.

### 5.6. Spatial Distribution of Maximum Accelerations

A comprehensive investigation of the spatial distribution of peak accelerations along the longitudinal and lateral dimensions of the bridge can be ascertained from the depictions in Figures 21 and 22. These figures illustrate the maximum recorded acceleration values obtained from each sensor (accelerometers A and C at  $L/2$ , B at  $L/4$ , and D at  $3L/4$ , where B, C, and D are located at mid-width, and A is located at the cantilever side) during the three different crossings (normal walk at 2 Hz, random walk, and normal run at 3.67 Hz) exerted by pedestrian A and a group consisting of nine pedestrians. It is shown that for the case of pedestrian A, accelerometer C was recording the most intensified response while disturbing the bridge with the three different frequencies in both directions, revealing a symmetric response for sensors at quarter-edges with respect to the sensors at mid-length. Conversely, for the case of the nine pedestrians, it is shown that accelerometers B and D record higher acceleration than accelerometer C, as shown in the results of a random run scenario in the vertical direction. Moreover, the results of only one of the quarter-edge sensors can exceed that of the mid-length, addressing an asymmetric response, as is shown in the result of a random walk scenario in the lateral direction. This is due to unsynchronized footsteps of numerous pedestrians taking more time to adjust their movement with their neighbors while crossing the bridge. Then, the whole crowd readjust their pace to harmonize with the that of the bridge. For both cases of one and nine pedestrians and at any disturbance frequency, accelerometer C always records a higher acceleration intensity than accelerometer A. It is noteworthy that, in the vertical direction, a maximum acceleration of  $1.5 \text{ m/s}^2$  was reported for both cases of one pedestrian and a crowd.

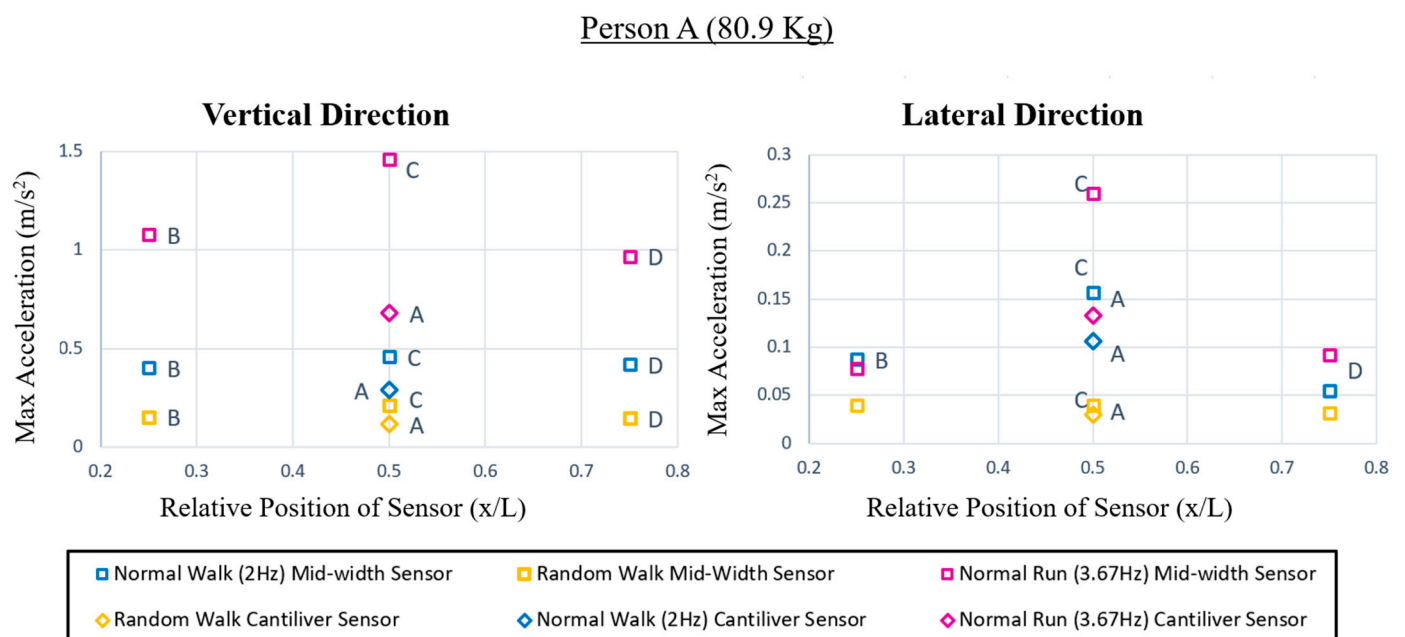


**Figure 21.** Spatial distribution of maximum accelerations as pedestrian A crosses along the bridge length.

### 5.7. Comfort Level Control

The level of comfort is assessed by comparing the maximum recorded accelerations on different crossings with the limits of the regulation and by directly recording the subjective feeling of the test participants.

Table 6 presents the limit values of accelerations as defined by EN 1990–A2 [48], and the SETRA [44] directives based on which level of comfort, in the pedestrian bridge under study, was evaluated.

9 People (791.2 Kg)

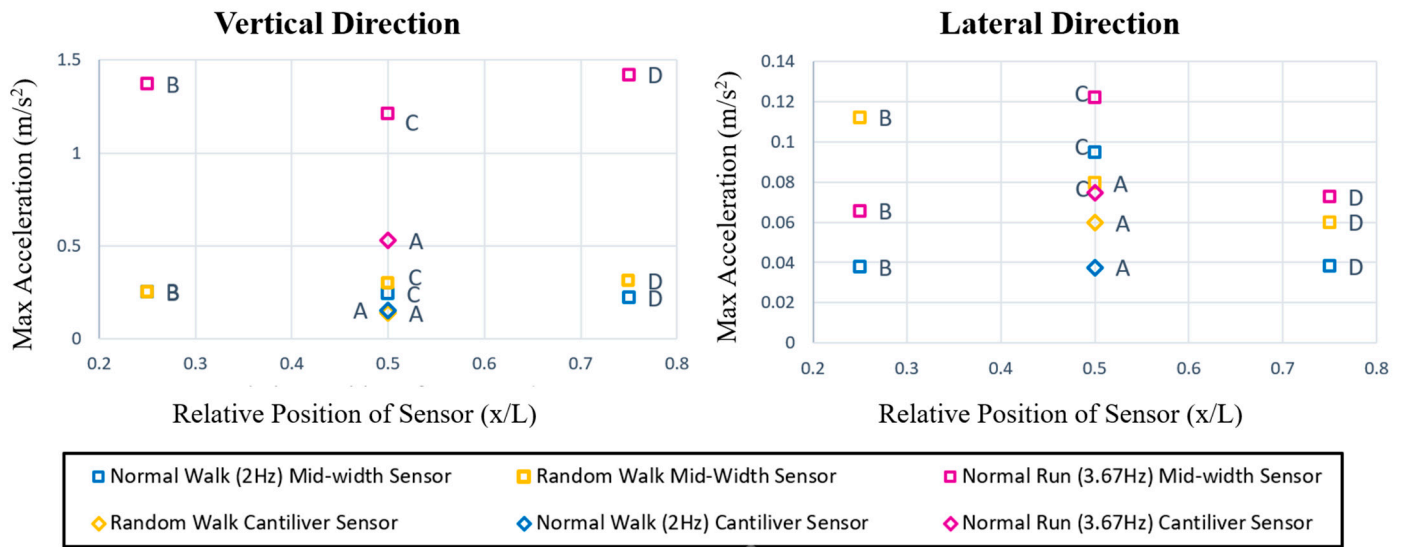


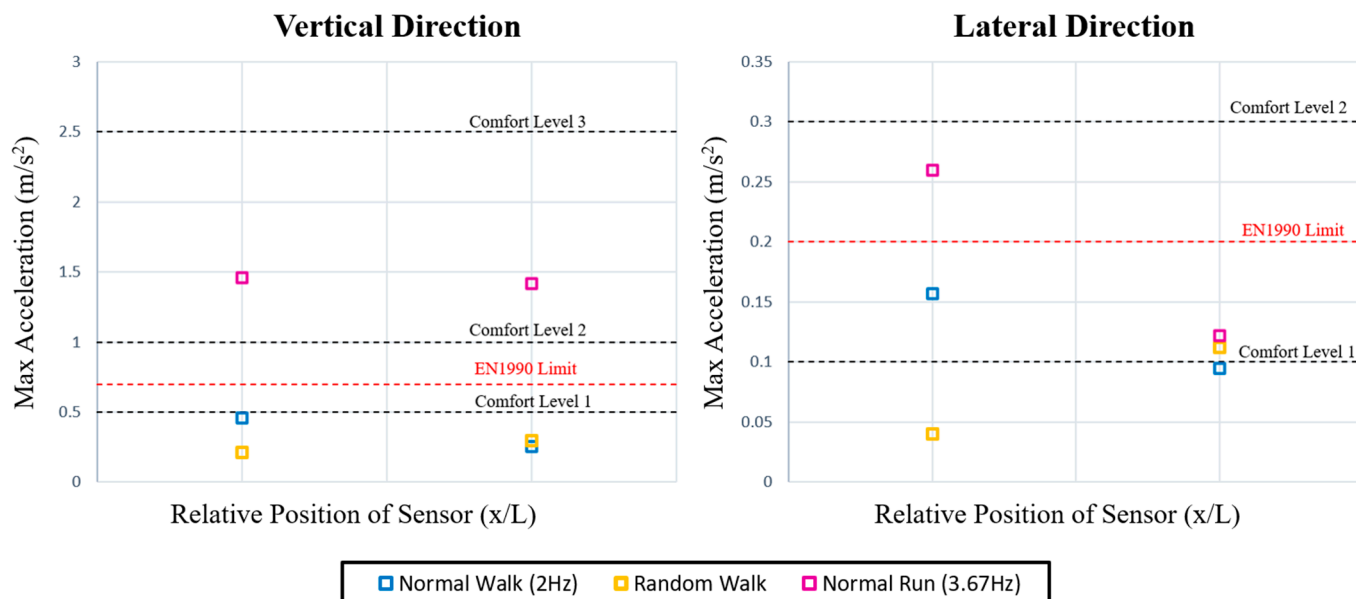
Figure 22. Spatial distribution of maximum accelerations as the 9-pedestrian group crosses along the bridge length.

Table 6. Maximum allowable accelerations based on specifications.

Comfort Level	Degree of Comfort	Acceleration [m/s <sup>2</sup> ]			
		Vertical Direction		Lateral Direction	
		EN 1990	SETRA	EN 1990	SETRA
1	Maximum	0.7	<0.5	0.2	<0.1
2	Medium		0.5–1.0		0.1–0.3
3	Minimum		1.0–2.5		0.3–0.8
4	Not acceptable		>2.5		>0.8

Figure 23 compares the maximum accelerations recorded by one individual and group pedestrian crossings for each type of walk. The differences in accelerations between people for almost all crossings are evident in both directions. However, there is no apparent ratio between pedestrian weight and deployed acceleration, leading to the conclusion that the amount of acceleration recorded when pedestrians cross depend on other biometric characteristics.

The limit values for accelerations, as defined in the specifications, are also indicated in the same figure. It should be noted that for all passages, the developing accelerations are classified at the maximum comfort level on the basis of specifications in both vertical and lateral directions. The exceptions are the crossings of pedestrian A and the group of nine pedestrians running with a frequency equal to the first vertical frequency of the 3.67 Hz bridge where vertical accelerations are at medium comfort levels.



**Figure 23.** Maximum vertical and horizontal accelerations for each type of walking from individual pedestrian and group of 9 pedestrians.

## 6. Conclusions

In conclusion, this paper presented the use of a computer-based data acquisition system and an automated coding software, LabVIEW, for structural health monitoring and system identification of a real-time pedestrian bridge located in Haidari, Greece, after the completion of construction. It calculated its dynamic properties, and characterized its comfort level.

Dynamic properties were found to have three eigenfrequencies of 3.67, 7.62, and 10.22 Hz in the vertical direction, with a damping of 2.25% for the first and 1.45% for the second eigenfrequency. For the lateral direction, the three detected eigenfrequencies were 6.18, 7.62, and 10.22 Hz. And a damping of 1.93% for the first and 1.14% for the second eigenfrequency were found. For each eigenfrequency, a distinct mode shape was found.

As safety was proven, the comfort level was tested as pedestrians crossed according to EN 1990, A.2.4.3.2 [48]. The results demonstrated comfort in crossing the bridge in both directions until a limit of 3.67 Hz running activity was reached, where the bridge absorbed the dissipated energy from the pedestrians by vibrating for seconds to finally restore to its initial posture.

It is concluded that the bridge excitations during pedestrian crossing are within the specifications and do not require the installation of dampers. But it is recommended to avoid malicious use of the bridge.

**Supplementary Materials:** The following supporting information can be downloaded at: <https://www.mdpi.com/article/10.3390/buildings13123053/s1>.

**Author Contributions:** Conceptualization, R.E.D.; Methodology, R.E.D. and I.V.; Software, R.E.D., X.L. and S.P.; Validation, R.E.D., X.L., I.V. and S.P.; Formal Analysis, R.E.D.; Writing—Original Draft, R.E.D.; Writing—Review and Editing, I.V.; Supervision, I.V. All authors have read and agreed to the published version of the manuscript.

**Funding:** This research received no external funding.

**Data Availability Statement:** The data presented in this study are available in Supplementary Materials.

**Conflicts of Interest:** The authors declare no conflict of interest.

## References

1. Lu, P.; Zhou, Y.; Wu, Y.; Li, D.; Zhou, C. Vibration reduction using tuned mass dampers in composite steel box girder footbridge with self-anchored suspension. *Int. J. Struct. Stab. Dyn.* **2021**, *21*, 2150110. [[CrossRef](#)]
2. Caprani, C.C.; Ahmadi, E. Formulation of human–structure interaction system models for vertical vibration. *J. Sound Vib.* **2016**, *377*, 346–367. [[CrossRef](#)]
3. Morichika, S.; Sekiya, H.; Zhu, Y.; Hirano, S.; Maruyama, O. Estimation of displacement response in steel plate girder bridge using a single MEMS accelerometer. *IEEE Sens. J.* **2021**, *21*, 8204–8208. [[CrossRef](#)]
4. Liu, Y.; Bao, Y. Review of electromagnetic waves-based distance measurement technologies for remote monitoring of civil engineering structures. *Measurement* **2021**, *176*, 109193. [[CrossRef](#)]
5. Gao, J.; Li, D.; Feng, Y.; Wan, L.; Wu, G. Application and Research of Health Monitoring System of Xiangshan Port Bridge. In Proceedings of the IOP Conference Series: Earth and Environmental Science, Nanchang, China, 12 April 2021; IOP Publishing: Bristol, UK; Volume 719, p. 032098.
6. Ko, J.M.; Ni, Y.Q. Technology developments in structural health monitoring of large-scale bridges. *Eng. Struct.* **2005**, *27*, 1715–1725. [[CrossRef](#)]
7. Li, H.N.; Li, D.S.; Song, G.B. Recent applications of fiber optic sensors to health monitoring in civil engineering. *Eng. Struct.* **2004**, *26*, 1647–1657. [[CrossRef](#)]
8. Caicedo, J.M.; Marulanda, J.; Thomson, P.; Dyke, S.J. Monitoring of bridges to detect changes in structural health. In Proceedings of the 2001 American Control Conference, Arlington, VA, USA, 25–27 June 2001; IEEE: Piscataway, NJ, USA; Volume 1 (Cat. No. 01CH37148), pp. 453–458. [[CrossRef](#)]
9. Li, Z.X.; Chan, T.H.; Ko, J.M. Fatigue analysis and life prediction of bridges with structural health monitoring data—Part I: Methodology and strategy. *Int. J. Fatigue* **2001**, *23*, 45–53. [[CrossRef](#)]
10. Basharat, A.; Catbas, N.; Shah, M. A framework for intelligent sensor network with video camera for structural health monitoring of bridges. In Proceedings of the Third IEEE International Conference on Pervasive Computing and Communications Workshops, Kauai, HI, USA, 8–12 March 2005; IEEE: Piscataway, NJ, USA; pp. 385–389. [[CrossRef](#)]
11. Park, K.T.; Kim, S.H.; Park, H.S.; Lee, K.W. The determination of bridge displacement using measured acceleration. *Eng. Struct.* **2005**, *27*, 371–378. [[CrossRef](#)]
12. Peeters, B.; Maeck, J.; De Roeck, G. Vibration-based damage detection in civil engineering: Excitation sources and temperature effects. *Smart Mater. Struct.* **2001**, *10*, 518. [[CrossRef](#)]
13. Matsuoka, K.; Collina, A.; Somaschini, C.; Sogabe, M. Influence of local deck vibrations on the evaluation of the maximum acceleration of a steel-concrete composite bridge for a high-speed railway. *Eng. Struct.* **2019**, *200*, 109736. [[CrossRef](#)]
14. Bačinskas, D.; Kamaitis, Z.; Kilikevičius, A. A sensor instrumentation method for dynamic monitoring of railway bridges. *J. Vibroeng.* **2013**, *15*, 176–184.
15. Brownjohn, J.M.W.; De Stefano, A.; Xu, Y.L.; Wenzel, H.; Aktan, A.E. Vibration-based monitoring of civil infrastructure: Challenges and successes. *J. Civil. Struct. Health Monit.* **2011**, *1*, 79–95. [[CrossRef](#)]
16. Xia, H.; Zhang, N.; Gao, R. Experimental analysis of railway bridge under high-speed trains. *J. Sound Vib.* **2005**, *282*, 517–528. [[CrossRef](#)]
17. Chaudhari, P.K.; Patel, D.; Patel, V. Theoretical and software-based comparison of cantilever beam: Modal analysis. *Int. J. Innov. Res. Adv. Eng.* **2014**, *1*, 75–79.
18. Xia, Y.; Li, H.; Fan, Z.; Xiao, J. Modal parameter identification based on hilbert vibration decomposition in vibration stability of bridge structures. *Adv. Civ. Eng.* **2021**, *2021*, 6688686. [[CrossRef](#)]
19. Pirskaewitz, S.M.; Schmidt, S. Detection of wire breaks in prestressed concrete bridges by Acoustic Emission analysis. *Dev. Built Environ.* **2023**, *14*, 100151. [[CrossRef](#)]
20. Doebling, S.W.; Farrar, C.R.; Prime, M.B.; Shevitz, D.W. *Damage Identification and Health Monitoring of Structural and Mechanical Systems from Changes in Their Vibration Characteristics: A Literature Review*; USDOE: Washington, DC, USA, 1996. [[CrossRef](#)]
21. Gentile, C.; Saisi, A. Ambient vibration testing of historic masonry towers for structural identification and damage assessment. *Constr. Build. Mater.* **2007**, *21*, 1311–1321. [[CrossRef](#)]
22. Gentile, C.; Saisi, A.; Cabboi, A. Structural identification of a masonry tower based on operational modal analysis. *Int. J. Archit. Herit.* **2015**, *9*, 98–110. [[CrossRef](#)]
23. Foti, D. Non-destructive techniques and monitoring for the evolutive damage detection of an ancient masonry structure. *Key Eng. Mater.* **2015**, *628*, 168–177. [[CrossRef](#)]
24. Lacanna, G.; Ripepe, M.; Coli, M.; Genco, R.; Marchetti, E. Full structural dynamic response from ambient vibration of Giotto’s bell tower in Firenze (Italy), using modal analysis and seismic interferometry. *NDT E Int.* **2019**, *102*, 9–15. [[CrossRef](#)]
25. Bayraktar, A.; Türker, T.; Altunişik, A.C. Experimental frequencies and damping ratios for historical masonry arch bridges. *Constr. Build. Mater.* **2015**, *75*, 234–241. [[CrossRef](#)]
26. González, A.; Feng, K.; Casero, M. Effective separation of vehicle, road and bridge information from drive-by acceleration data via the power spectral density resulting from crossings at various speeds. *Dev. Built Environ.* **2023**, *14*, 100162. [[CrossRef](#)]
27. Zäll, E.; Andersson, A.; Ülker-Kaustell, M.; Karoumi, R. An efficient approach for considering the effect of human-structure interaction on footbridges. *Procedia Eng.* **2017**, *199*, 2913–2918. [[CrossRef](#)]

28. Živanović, S. Modelling human actions on lightweight structures: Experimental and numerical developments. In Proceedings of the MATEC Web of Conferences, Dübendorf (Zürich), Switzerland, 19–21 October 2015; EDP Sciences: Les Ulis, France; Volume 24. [\[CrossRef\]](#)
29. Dallard, P.; Fitzpatrick, T.; Flint, A.; Low, A.; Smith, R.R.; Willford, M.; Roche, M. London Millennium Bridge: Pedestrian-induced lateral vibration. *J. Bridge Eng.* **2001**, *6*, 412–417. [\[CrossRef\]](#)
30. Willford, M. Solving the vibration problems of the London Millennium footbridge. In *Schwingungen in der Baupraxis: 12*; Dresdner Baustatik-Seminar: Dresden, Germany, 2008; pp. 157–179.
31. Wieczorek, N.; Gerasch, W.J.; Rolfes, R.; Kammerer, H. Semiactive friction damper for lightweight pedestrian bridges. *J. Struct. Eng.* **2014**, *140*, 04013102. [\[CrossRef\]](#)
32. Jones, R.T.; Pretlove, A.J. Two case studies in the use of tuned vibration absorbers on foot bridges. *Struct. Engineer. Part B* **1981**, *59*, 27–32. Available online: <http://worldcat.org/issn/00392553> (accessed on 16 September 2023).
33. Caetano, E.; Cunha, Á.; Magalhães, F.; Moutinho, C. Studies for controlling human-induced vibration of the Pedro e Inês footbridge, Portugal. Part 1: Assessment of dynamic behaviour. *Eng. Struct.* **2010**, *32*, 1069–1081. [\[CrossRef\]](#)
34. Caetano, E.; Cunha, Á.; Moutinho, C.; Magalhães, F. Studies for controlling human-induced vibration of the Pedro e Inês footbridge, Portugal. Part 2: Implementation of tuned mass dampers. *Eng. Struct.* **2010**, *32*, 1082–1091. [\[CrossRef\]](#)
35. Tubino, F.; Carassale, L.; Piccardo, G. Human-induced vibrations on two lively footbridges in Milan. *J. Bridge Eng.* **2016**, *21*, C4015002. [\[CrossRef\]](#)
36. Feng, P.; Wang, Z.; Jin, F.; Zhu, S. Vibration serviceability assessment of pedestrian bridges based on comfort level. *J. Perform. Constr. Facil.* **2019**, *33*, 04019046. [\[CrossRef\]](#)
37. Wright, D.T.; Green, R. *Human Sensitivity to Vibration*; No. 7; Queen’s University: Kingston, ON, Canada, 1959.
38. Smith, J.W. *Vibration of Structures: Applications in Civil Engineering Design*; Chapman & Hall: New York, NY, USA, 1988.
39. Wheeler, J.E. Prediction and control of pedestrian-induced vibration in footbridges. *J. Struct. Div.* **1982**, *108*, 2045–2065. [\[CrossRef\]](#)
40. Dey, P.; Narasimhan, S.; Walbridge, S. Evaluation of design guidelines for the serviceability assessment of aluminum pedestrian bridges. *J. Bridge Eng.* **2017**, *22*, 04016109. [\[CrossRef\]](#)
41. Anon, B. *SS ISO 2631(1)*; Mechanical Vibration and Shock-Evaluation of HUMAN Exposure to Whole-Body Vibration. International Organization for Standardization: Geneva, Switzerland, 1997.
42. Wang, W.; Yan, W.; Deng, L.; Kang, H. Dynamic analysis of a cable-stayed concrete-filled steel tube arch bridge under vehicle loading. *J. Bridge Eng.* **2015**, *20*, 04014082. [\[CrossRef\]](#)
43. Feldman, M. *HiVOSS—Human-Induced Vibrations of Steel Structures-Design of Footbridges: Guideline*; Office for Official Publications of the European Communities: Luxembourg, 2008. Available online: <http://www.stb.rwth-aachen.de/projekte/2007/HIVOSS/download.php.ISO> (accessed on 20 April 2023).
44. *Sétra—Service D’études sur les Transports, les Routes et Leurs Aménagements*; Assessment of Vibrational Behaviour of Footbridges under Pedestrian Loading; Technical Guide; Sétra: Paris, France, 2006. Available online: [https://www.academia.edu/40689257/S%25C3%25A9tra\\_Footbridges\\_Assessment\\_of\\_vibrational\\_behaviour\\_of\\_footbridges\\_under\\_pedestrian\\_loading](https://www.academia.edu/40689257/S%25C3%25A9tra_Footbridges_Assessment_of_vibrational_behaviour_of_footbridges_under_pedestrian_loading) (accessed on 20 April 2023).
45. Van Nimmen, K.; Lombaert, G.; De Roeck, G.; Van den Broeck, P. Vibration serviceability of footbridges: Evaluation of the current codes of practice. *Eng. Struct.* **2014**, *59*, 448–461. [\[CrossRef\]](#)
46. El Dahr, R.; Lignos, X.; Papavarios, S.; Vayas, I. Design and Validation of an Accurate Low-Cost Data Acquisition System for Structural Health Monitoring of a Pedestrian Bridge. *J. Civ. Eng. Constr.* **2022**, *11*, 113–126. [\[CrossRef\]](#)
47. El Dahr, R.; Lignos, X.; Papavarios, S.; Vayas, I. Development and Validation of a LabVIEW Automated Software System for Displacement and Dynamic Modal Parameters Analysis Purposes. *Modelling* **2023**, *4*, 189–210. [\[CrossRef\]](#)
48. EN 1990 (English): Eurocode—Basis of Structural Design; Authority: The European Union Per Regulation 305/2011, Directive 98/34/EC, Directive 2004/18/EC. 2002. Available online: <https://www.phd.eng.br/wp-content/uploads/2015/12/en.1990.2002.pdf> (accessed on 20 April 2023).
49. Hinrichsen, P.F. Acceleration, velocity, and displacement for magnetically damped oscillations. *Phys. Teach.* **2019**, *57*, 250–253. [\[CrossRef\]](#)

**Disclaimer/Publisher’s Note:** The statements, opinions and data contained in all publications are solely those of the individual author(s) and contributor(s) and not of MDPI and/or the editor(s). MDPI and/or the editor(s) disclaim responsibility for any injury to people or property resulting from any ideas, methods, instructions or products referred to in the content.